

## Cages and Anomalous Diffusion in Vibrated Dense Granular Media

Camille Scalliet

*Université de Lyon, Ecole Normale Supérieure de Lyon, Laboratoire de physique,  
46 Allée d'Italie, 69364 Lyon, Cedex 07, France  
and Dipartimento di Fisica, Università "Sapienza", Piazzale Aldo Moro 5, 00185 Rome, Italy*

Andrea Gnoli and Andrea Puglisi

*Istituto dei Sistemi Complessi-Consiglio Nazionale delle Ricerche, 00185 Rome, Italy  
and Dipartimento di Fisica, Università "Sapienza", Piazzale Aldo Moro 5, 00185 Rome, Italy*

Angelo Vulpiani

*Dipartimento di Fisica, Università "Sapienza", Piazzale Aldo Moro 5, 00185 Rome, Italy  
and Istituto dei Sistemi Complessi-Consiglio Nazionale delle Ricerche, 00185 Rome, Italy  
(Received 12 September 2014; published 15 May 2015)*

A vertically shaken granular medium hosts a blade rotating around a fixed vertical axis, which acts as a mesorheological probe. At high densities, independently of the shaking intensity, the blade's dynamics shows strong caging effects, marked by transient subdiffusion and a maximum in the velocity power density spectrum, at a resonant frequency  $\sim 10$  Hz. Interpreting the data through a diffusing harmonic cage model allows us to retrieve the elastic constant of the granular medium and its collective diffusion coefficient. For high frequencies  $f$ , a tail  $\sim 1/f$  in the velocity power density spectrum reveals nontrivial correlations in the intracage microdynamics. At very long times (larger than 10 s), a superdiffusive behavior emerges, ballistic in the most extreme cases. Consistently, the distribution of slow velocity inversion times  $\tau$  displays a power-law decay, likely due to persistent collective fluctuations of the host medium.

DOI: 10.1103/PhysRevLett.114.198001

PACS numbers: 45.70.-n, 05.40.-a, 47.57.Gc

A comprehensive theory of dense granular media is still lacking [1]. Unperturbed granular systems may support external forces without flowing, behaving like a solid: in this configuration, a granular packing may show an elastic response to small stresses. Under gentle tapping, the granular medium undergoes very slow rearrangements, which resemble the sluggish response of molecular glasses [2–5]. The jamming transition, observed when reducing the vibration intensity, or increasing the density, is commonly compared to the glass transition in undercooled liquids [6]. When the energy of the external vibration is increased or the density is decreased, the granular medium enters a liquidlike phase [7], which has not received as much attention as the glass or solid phases or the much more dilute gas phase [8]. Nevertheless, learning from molecular fluids, the dynamics of the liquid phase is rich in information: in particular, it gives important hints about the many time scales developing when the glass transition is approached from above [9]. Recent theoretical and experimental insights into the liquid phase have highlighted the differences between molecular glass formers and driven granular media, in particular the presence of superdiffusive behavior [10–13].

As rheometers are usually conceived to apply the excitation at the boundaries, standard rheology in granular liquids is typically limited by problems of slip and shear localization. Other techniques exist to probe the bulk response properties of granular media, e.g., magnetic

resonance imaging, x-ray tomography, and high-speed particle tracking [14], confocal microscopy [15], or multi-speckle dynamic light scattering [11]. Microrheology [16] is also used, e.g., to probe transient subdiffusive behavior and cage effects [17]. However, the ability of small intruders to probe the collective behavior at large spatial scales in the host granular medium is not evident.

We propose a technique, which could be named passive mesorheology, see Fig. 1(a), inspired from previous works [7,18–20]. The granular medium made of spheres of

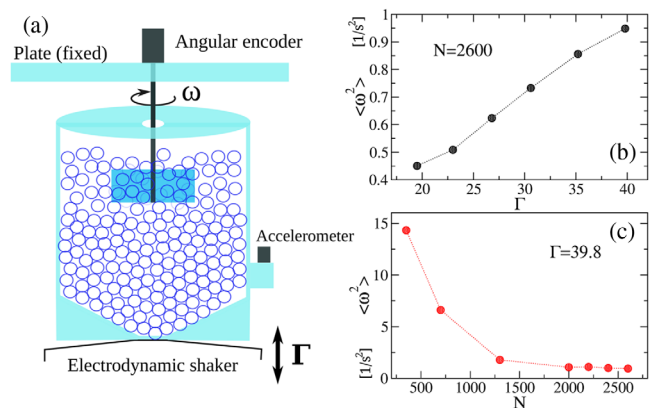


FIG. 1 (color online). (a) Schematic of the experimental setup. (b),(c) Mean squared angular velocity of the blade in the various experiments.

diameter  $d = 4$  mm is placed in a cylindrical container of volume  $\sim 7300$  times that of a sphere. The container is vertically shaken with a signal whose spectrum is approximately flat in a range  $[f_{\min}, f_{\max}]$  with  $f_{\min} = 200$  Hz and  $f_{\max} = 400$  Hz. A blade, our probe with a cross section  $\sim 8d \times 4d$  and momentum of inertia  $I$ , is suspended into the granular medium and rotates around a vertical axis. Its angular velocity  $\omega(t)$  and the traveled angle of rotation  $\theta(t) = \int_0^t \omega(t') dt'$  are measured with a time resolution of 2 kHz. The blade, interacting with the spheres, performs a motion qualitatively similar to an angular Brownian motion. Two families of experiments have been performed: (a) a series at high density ( $N = 2600$ ), varying the shaking intensity  $\Gamma = \dot{z}_{\max}/g \in [19.5, 39.8]$ , and (b) a series at high shaking intensity ( $\Gamma = 39.8$ ), varying  $N \in [300, 2600]$  and the packing fraction  $\phi$  as indicated in the figures. Figures 1(b) and 1(c) report the values of the mean squared angular velocity  $\langle \omega^2 \rangle$  of the blade in the different experiments. Details on dimensions of the setup and shaking parameters are reported in the Supplemental Material [21].

*Velocity power density spectrum.*—In Fig. 2, we present our main results in the form of the velocity power density spectrum (VPDS) of the velocity signal  $\omega(t)$ , which is defined as  $S(f) = (1/2\pi t_{\text{TOT}}) |\int_0^{t_{\text{TOT}}} \omega(t) e^{i(2\pi f)t} dt|^2$ . We recognize four frequency ranges, denoted as regions I, II, III, and IV. In the experiments at fixed (maximum) density,  $N = 2600$ , displayed in Fig. 2(a), the spectrum conserves the same qualitative shape, vertically shifted due to the differences in  $\Gamma$ . The most striking properties are observed in regions II and III:  $S(f)$  goes from a plateau in region II to a roughly parabolic maximum centered at a frequency  $f^*$  in region III. The value of the resonant frequency  $f^*$  slightly shifts from 10 to 20 Hz as  $\Gamma$  decreases. To avoid interference, we ensured that the shaker vibration is in a distant region (200–400 Hz); we changed such a range (including trials with a single frequency, i.e., a harmonic vibration), obtaining always the same shape  $S(f)$  with the same values of  $f^*$ . A mechanical resonance is also observed at  $\sim 70$  Hz, due to the nonperfect acoustic insulation of the plate on which the couple encoder or blade is mounted. In conclusion, the maximum in  $f^*$  is a resonance experienced by the blade in its motion through the granular medium, and we interpret it as a transient trapping phenomenon, analogous to caging effects in low-temperature or high-density liquids. We will see that such an interpretation is well supported by other observations and by a theoretical model. In both “extremal” regions I and IV,  $S(f)$  is a decreasing function of  $f$ . In particular, in region IV, the high-frequency decay presents a power law  $\sim f^{-\beta}$  with  $1 < \beta < 2$ , close to 1 for the lowest values of  $\Gamma$ . This is evidence of collective effects, in the fast processes inside a cage (as  $f \gg f^*$ ), occurring without a characteristic frequency [22]. The decay in region I is also anomalous and denotes the emergence of long characteristic times, possibly larger than the experiment duration

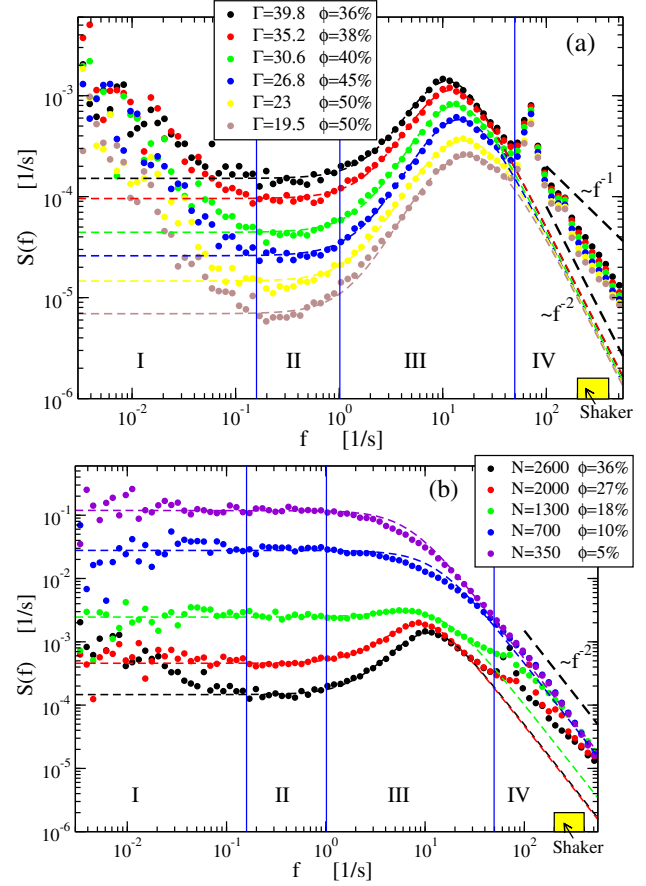


FIG. 2 (color online). Power density spectra of the blade’s angular velocity for the two series. (a) The number of beads is fixed ( $N = 2600$ ) and the shaking intensity varies. (b) The shaking intensity is fixed to  $\Gamma = 39.8$  and  $N$  changes. The frequencies of vibration are marked by the yellow bar. Dashed lines are fits of Eq. (2) to the experimental data in regions II and III. Thick-dashed lines show the limit behaviors  $f^{-2}$  and  $f^{-1}$ .

$t_{\text{TOT}} = 3600$  s. Note that the asymptotic diffusion is governed by  $\lim_{t \rightarrow \infty} \langle \Delta \theta^2(t) \rangle / t \sim 2\pi S(f \rightarrow 0)$ ; therefore, an increasing value of  $S(f)$  as  $f \rightarrow 0$  (i.e., at increasing time) indicates a superdiffusive behavior, detailed below.

When the density is reduced, see Fig. 2(b), the shape of  $S(f)$  drastically changes. The slope of the decay in region I decreases and eventually vanishes: at low densities a plateau spans both regions I and II. The maximum in region III is reduced and disappears for  $N < 1000$ , called the “gas” phase. The exponent of the power-law decay in region IV increases,  $\beta \rightarrow 2$ . The whole spectrum at the lowest densities is well fit by the Lorentzian  $S(f) = (T/\pi\gamma) / [1 + (2\pi I f / \gamma)^2]$ , expected for diffusion in diluted gases at temperature  $T$  with a collision frequency  $\propto \gamma$  [23]. Here  $T$  is the probe’s “kinetic temperature”  $T = I \langle \omega^2 \rangle$ .

*Mean-square displacement.*—The several phenomena observed in  $S(f)$  are reflected in the diffusion properties, see Fig. 3, where the mean-square displacement (MSD)

$\langle[\Delta\theta(t)]^2\rangle$  after a time  $t$  is plotted. The four temporal regions corresponding to the frequency regions discussed above are marked on the graph. Our “cagelike” interpretation of the maximum of  $S(f)$  in region III is corroborated, in Fig. 3(a), by the dramatic slowing down of  $\langle[\Delta\theta(t)]^2\rangle$  in the same region [24], resembling the typical dynamical slowdown in the diffusion of tracers dispersed in viscous liquids. At small times (region IV) the usual ballistic behavior appears. More remarkable is the behavior at large times. All the experiments with  $N = 2600$  present a superdiffusive range  $\sim t^\alpha$  in region II, with  $\alpha > 1$ . For the largest values of  $\Gamma$ , this behavior changes to a diffusive behavior  $\sim t$  in region I. On the contrary, at lower  $\Gamma$ , the superdiffusive exponent  $\alpha > 1$  remains the same as that of region II at large times. In particular, for  $\Gamma < 31$ , we find an almost ballistic superdiffusion,  $\alpha \sim 2$ . The situation is very different when the density is reduced [Fig. 3(b)]: the long time behavior (region I) is always of the normal type  $\sim t$ . In the most dilute cases ( $N < 1000$ ) the typical scenario of diffusion in a gaslike fluid is fully recovered in the form of a monotonic crossover from the ballistic region IV to the normal diffusion of regions II and I. Changing the size and

shape of the blade, see Ref. [21], does not lead to relevant changes in the above scenario.

The study of the VPDS and MSD is consistent with measurements of the velocity-autocorrelation function (VACF)  $C(t)$ , which is the inverse Fourier transform of  $S(f)$ . In the very dilute cases, it is close to a simple exponential decay. The most dense and “cold” experiments, on the contrary, reveal a VACF with many features: a fast, though nonexponential, decay at small times, followed by a backscattering oscillation through negative values, interpreted as the “cage,” and finally a slow decay to zero [25]. The final decay of the VACF could also shed light on the origin of the superdiffusion. Unfortunately, at large times the VACF is exceedingly noisy. A more promising way to probe long memory effects is to measure the times of persistency, i.e., the times during which the signal remains positively correlated. Our operative definition consists in two basic steps: (1) filtering out high frequency oscillations that are not relevant to the behavior at large times of  $\Delta\theta(t)$ , by taking the running average  $\omega_s(t) = (1/\tau) \int_t^{t+\tau} \omega(t') dt'$  over a large time  $\tau \geq 1$  s, and then (2) computing the statistics of the times separating two consecutive zeros of  $\omega_s(t)$ , which we call the inversion time  $t_{\text{inv}}$ ; see Figs. 4(a) and 4(b) for experimental samples of  $\omega(t)$ ,  $\omega_s(t)$ , and  $t_{\text{inv}}$ . The statistics of  $t_{\text{inv}}$  is a natural measurement of the long

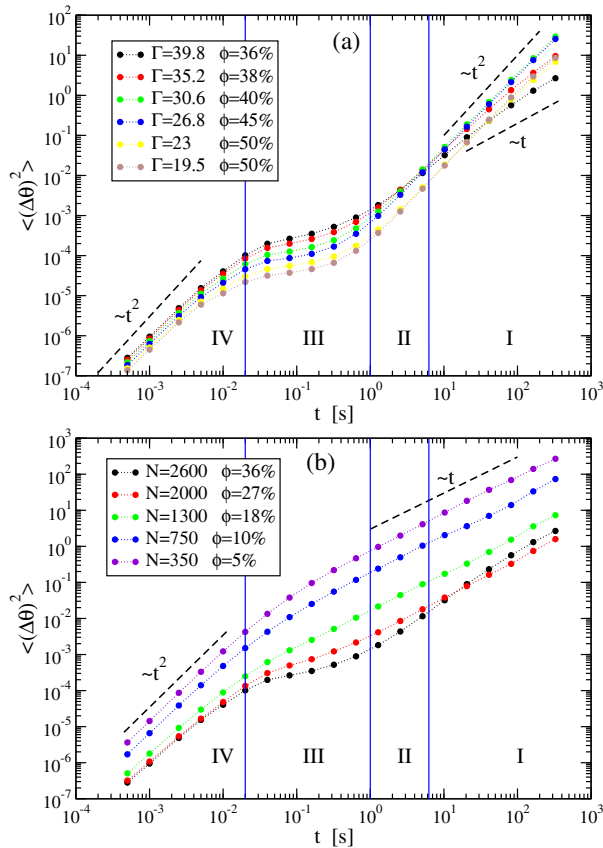


FIG. 3 (color online). Mean-squared displacement  $\langle[\Delta\theta(t)]^2\rangle$  after a time  $t$  for the two series. (a)  $N = 2600$  and  $\Gamma$  varies. (b) The shaking intensity is fixed to  $\Gamma = 39.8$  and  $N$  changes. Black dashed lines are guides for the eye.

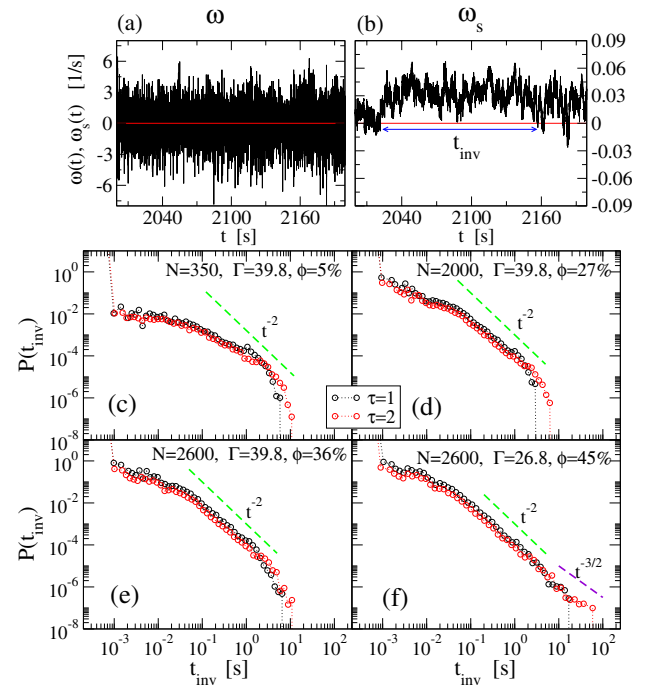


FIG. 4 (color online). (a),(b) Angular velocity  $\omega(t)$  and filtered signal  $\omega_s(t)$  (with a running average over a time  $\tau = 2$  s), for  $N = 2600$  and  $\Gamma = 26.8$ . (c)–(f) PDF of the inversion times calculated (with  $\tau = 1$  and 2 s) in different experiments. From (c)–(f) the following configurations are displayed: very dilute, intermediate, dense at high energy, dense at low energy. Colored dashed lines are guides for the eye.

term memory of the signal. The experimental probability density function (PDF) of  $t_{\text{inv}}$  is shown in Figs. 4(c)–4(f) for a few choices of parameters and values of  $\tau$ . We observe that it rapidly decays with an exponential cutoff smaller than or equal to  $\sim 10$  s in all cases where the MSD asymptotically showed normal diffusion, signaling a finite memory of the dynamics. The cutoff apparently jumps to a much larger value in the cases where the MSD displays superdiffusion: in such cases, the PDF decays to zero as a power  $\sim -2$  or even slower. This is fair evidence that long memory effects arise together with the observed superdiffusion. Long memory may be due to a slow, rotating, creeping motion of the surrounding granular medium, which acts as a coherent block and drags the blade. Such a “secondary” motion has long relaxation times due to the involved large inertia. New experiments are being designed with the aim of demonstrating this picture. We mention that longer experiments (shown in the Supplemental Material [21]) still display a superdiffusion that evolves in normal diffusion after many hours.

*Modeling the dynamics of the blade.*—In the most dense and cold experiments, the VPDS and the MSD display an intriguing superposition of phenomena over almost 6 decades of time scales. It seems hopeless to reduce such a complexity to a model with a simple physical interpretation. It is tempting to disentangle the two main phenomena, i.e., caging (occurring at times smaller than  $10^{-1}$  s) and superdiffusion (more evident at times larger than 10 s), by decomposing the dynamics into a slow and a fast component  $\omega(t) = \omega_s(t) + \omega_f(t)$ , with  $\omega_s(t)$  defined above. Experimental data demonstrate that the standard deviation of  $\omega_f(t)$  is much larger than that of  $\omega_s$  and therefore dominates at short times (large frequencies). At long times (small frequencies), on the contrary, the fast dynamics averages out and  $\omega_s(t)$  emerges as the leading signal. For the fast dynamics, we propose a simple interpretation of the transient caging phenomena through a “diffusing harmonic cage” model: this is a simplified version of the itinerant oscillator model describing translational and rotational diffusion of particles in liquids [26,27], and reads

$$\dot{\theta}(t) = \omega_f(t), \quad \dot{\theta}_0(t) = \sqrt{2D_0}\xi'(t), \quad (1a)$$

$$I\dot{\omega}_f(t) = -\gamma\omega_f(t) - K[\theta(t) - \theta_0(t)] + \sqrt{2\gamma T}\xi(t), \quad (1b)$$

where  $\xi(t)$  and  $\xi'(t)$  are white normal Gaussian noises. The model represents the diffusion of a particle in a harmonic potential with “stiffness”  $K$  and an unfixed minimum, under the effect of a thermal bath at temperature  $T$  and relaxation time  $I/\gamma$ . The harmonic potential, representing the cage due to the confining effect of the dense granular host fluid, is not fixed but moves, as  $\theta_0(t)$  behaves as Brownian motion with diffusivity  $D_0$ . Motivation for this model is twofold: (1) the main features of the VPDS, i.e., an elastic resonance (region III) and a plateau revealing loss of

memory at larger times (region II), and (2) that in the dilute limit it can be rigorously derived [28], while at intermediate densities a series of studies showed that memory effects (coming from correlated collisions) are well described by a coupling with an additional degree of freedom fluctuating at slower time scales [23]. The VPDS of the above model can be calculated and reads

$$S(f) = \frac{1}{\pi} \frac{D_0 K^2 + \gamma T (2\pi f)^2}{\gamma^2 (2\pi f)^2 + [K - I(2\pi f)^2]^2}. \quad (2)$$

Two limiting cases are recovered: when  $K = 0$ , the Ornstein-Uhlenbeck process is obtained, with  $S(f)$  taking the Lorentzian form mentioned before. When  $K > 0$  and  $D_0 = 0$ , one has the Klein-Kramers process in a fixed harmonic potential, and  $S(f) \rightarrow 0$  for  $f \rightarrow 0$ , expressing the absence of diffusion at large times: the cage does not move and fully confines the particle. Formula (2) fairly fits all experimental spectra in regions II and III, with parameters given in Tables 2 and 3 of Ref. [21]. Reasonably, the “cage stiffness” decreases at increasing shaking intensity. It also decreases as the density is reduced, and abruptly goes to zero for  $N \sim 1000$ . The “cage diffusivity”  $D_0$  rapidly increases with increasing  $\Gamma$  and with decreasing  $N$ . A more detailed study of the transition from the cage behavior  $K \neq 0$  to the free behavior  $K = 0$  is postponed for future investigations.

A more ambitious task is to devise a simple mechanism for  $\omega_s(t)$ , leading to superdiffusion. In driven granular systems it has been observed below the jamming transition [12] and in a few cases above it, where it was imputed to “zero” modes of the host fluid [10], to Taylor dispersion [13], or to turbulence-like cascade effects [29]. We stress that, at variance with standard diffusion, for anomalous diffusion there is nothing similar to universality [30]. A systematic derivation of anomalous diffusion is a hard task and it is possible only in few specific cases [30]. Of course, the basic ingredient must be an enduring memory: a way to achieve it is to replace standard time derivatives with fractional derivatives in the Fokker-Planck equations, an approach that is the subject of a vast literature [31]. Such an approach is capable, in principle, of describing both caging and superdiffusion within a single model equation, at the price of losing an immediate interpretation and plain calculations. In a complementary approach [32], a coarse-grained value of  $\omega_s(t)$  (where only the sign of this quantity is traced) follows a continuous time random walk (CTRW): it takes discrete values with random transition times extracted from a given distribution. A simplified version of the CTRW is discussed in the Supplemental Material [21]. We highlight that the CTRW gets a suggestive experimental confirmation in the observations of Fig. 4; indeed, the CTRW model quantitatively connects the observed slow decay of  $P(t_{\text{inv}})$  to superdiffusion.

*Conclusion.*—An experimental study of dense granular mesorheology allows us to probe time scales in a range of 6 orders of magnitude. Such an investigation reveals a complex scenario with different dynamical behaviors in four frequency or time regions. Three crucial features are observed at large density and low temperature: a “resonant” caging phenomenon at intermediate scales, nonwhite noise at fast scales, and superdiffusion at long times. The caging phenomenon is compatible with a diffusing harmonic cage model, while the superdiffusion seems to be rooted in the long inversion times appearing in the dynamics  $\omega_s(t)$ , possibly related to creeping rotating motion of the granular media. A more detailed investigation of transitions is in order: a gas-liquid transition could be put in evidence by studying how  $K \rightarrow 0$  when  $N$  decreases; a liquid-glass transition could be taking place at the lowest values of  $\Gamma$  or upon eventually increasing  $N > 2600$ . Superdiffusion and large values of  $t_{\text{inv}}$  could be signaling such a transition. Another promising line of investigation is active mesorheology, i.e., probing the response of the system to the application of an external force, achieved by coupling a controllable motor to the blade [19].

We wish to thank A. Lasanta Becerra and A. Sarracino for useful discussions. A. P. acknowledges the support of the Italian MIUR grants FIRB-IDEAS n. RBID08Z9JE.

- 
- [1] B. Andreotti, Y. Forterre, and O. Pouliquen, *Granular Media. Between Fluid and Solid* (Cambridge University Press, Cambridge, England, 2013).
- [2] R. A. Bagnold, *Proc. R. Soc. Lond. A* **225**, 49 (1954).
- [3] G. H. Wortel, J. A. Dijksman, and M. van Hecke, *Phys. Rev. E* **89**, 012202 (2014).
- [4] P. Wang, C. Song, and H. A. Makse, *Nat. Phys.* **2**, 526 (2006).
- [5] C. Song, P. Wang, and H. A. Makse, *Proc. Natl. Acad. Sci. U.S.A.* **102**, 2299 (2005).
- [6] M. van Hecke, *J. Phys. Condens. Matter* **22**, 033101 (2010).
- [7] G. D’Anna, P. Mayor, A. Barrat, V. Loreto, and F. Nori, *Nature (London)* **424**, 909 (2003).
- [8] N. V. Brilliantov and T. Pöschel, *Kinetic Theory of Granular Gases* (Oxford University Press, New York, 2004).
- [9] J. C. Dyre, *Rev. Mod. Phys.* **78**, 953 (2006).
- [10] C. Heussinger, L. Berthier, and J.-L. Barrat, *Europhys. Lett.* **90**, 20005 (2010).
- [11] L. Cipelletti, S. Manley, R. C. Ball, and D. A. Weitz, *Phys. Rev. Lett.* **84**, 2275 (2000).
- [12] F. Lechenault, O. Dauchot, G. Biroli, and J. P. Bouchaud, *Europhys. Lett.* **83**, 46003 (2008).
- [13] B. Utter and R. P. Behringer, *Phys. Rev. E* **69**, 031308 (2004).
- [14] D. M. Mueth, G. F. Debregeas, G. S. Karczmar, P. J. Eng, S. R. Nagel, and H. M. Jaeger, *Nature (London)* **406**, 385 (2000).
- [15] J. Brujić, C. Song, P. Wang, C. Briscoe, G. Marty, and H. A. Makse, *Phys. Rev. Lett.* **98**, 248001 (2007).
- [16] T. M. Squires and T. G. Mason, *Annu. Rev. Fluid Mech.* **42**, 413 (2010).
- [17] G. Marty and O. Dauchot, *Phys. Rev. Lett.* **94**, 015701 (2005).
- [18] A. L. Sellerio, D. Mari, G. Gremaud, and G. D’Anna, *Phys. Rev. E* **83**, 021301 (2011).
- [19] A. Gnoli, A. Puglisi, A. Sarracino, and A. Vulpiani, *PLoS One* **9**, e93720 (2014).
- [20] A. Naert, *Europhys. Lett.* **97**, 20010 (2012).
- [21] See Supplemental Material at <http://link.aps.org/supplemental/10.1103/PhysRevLett.114.198001> for details on the experimental setup, theory, and simulations.
- [22] M. B. Weissman, *Rev. Mod. Phys.* **60**, 537 (1988).
- [23] A. Sarracino, D. Villamaina, G. Gradenigo, and A. Puglisi, *Europhys. Lett.* **92**, 34001 (2010).
- [24] P. M. Reis, R. A. Ingale, and M. D. Shattuck, *Phys. Rev. Lett.* **98**, 188301 (2007).
- [25] A. Fiege, T. Aspelmeier, and A. Zippelius, *Phys. Rev. Lett.* **102**, 098001 (2009).
- [26] V. F. Sears, *Proc. Phys. Soc. London* **86**, 953 (1965).
- [27] W. Coffey, Yu. P. Kalmykov, and J. T. Waldron, *The Langevin Equation: With Applications in Physics, Chemistry, and Electrical Engineering* (World Scientific, Singapore, 1996).
- [28] A. Sarracino, D. Villamaina, G. Costantini, and A. Puglisi, *J. Stat. Mech.* (2010) P04013.
- [29] F. Radjai and S. Roux, *Phys. Rev. Lett.* **89**, 064302 (2002).
- [30] *Anomalous Transport*, edited by R. Klages, G. Radons, and I. M. Sokolov (Wiley&Sons, New York, 2008).
- [31] *Fractional Dynamics: Recent Advances*, edited by J. Klafter, S. C. Lim, and R. Metzler (World Scientific, Singapore, 2012).
- [32] K. H. Andersen, P. Castiglione, A. Mazzino, and A. Vulpiani, *Eur. Phys. J. B* **18**, 447 (2000).